Energy position of near-band-edge emission spectra of InN epitaxial layers with different doping levels

B. Arnaudov, T. Paskova, P. P. Paskov, B. Magnusson, E. Valcheva, and B. Monemar
Department of Physics and Measurements Technology, Linköping University, S-581 83 Linköping, Sweden

H. Lu and W. J. Schaff
Department of Electrical and Computer Engineering, Cornell University, Ithaca, New York 14853, USA

H. Amano and I. Akasaki
Department of Electrical and Electronic Engineering, Meijo University, I-501 Shiogamaguchi, Tempaku-ku, Nagoya 468, Japan
(Received 17 November 2003; published 30 March 2004)

We studied the shape and energy position of near-band-edge photoluminescence spectra of InN epitaxial layers with different doping levels. We found that the experimental spectra of InN layers with moderate doping level can be nicely interpreted in the frames of the ''free-to-bound'' recombination model in degenerate semiconductors. For carrier concentrations above $n>5\times10^{18}$ cm^{-3} the emission spectra can also be modeled satisfactorily, but a contribution due to a pushing up of nonequilibrium holes over the thermal delocalization level in the valence band tails should be considered in the model. The emission spectra of samples with low doping level were instead explained as a recombination from the bottom of the conduction band to a shallow acceptor assuming the same value of the acceptor binding energy estimated from the spectra of highly doped samples. Analyzing the shape and energy position of the free-electron recombination spectra we determined the carrier concentrations responsible for the emissions and found that the fundamental band gap energy of InN is $E_g=692\pm2$ meV for an effective mass at the conduction-band minimum $m_{n0}=0.042m_0$.

DOI: 10.1103/PhysRevB.69.115216 PACS number(s): 78.20.Bh, 81.05.Ea

For a very long time indium nitride has been regarded as a key material among group-III nitride semiconductors owing to its narrower band gap and smaller effective mass than those of AlN and GaN.[1] With the recent breakthrough in InN epitaxial technology and the discovery that the band gap of single-crystalline layers is much lower than 1.9 eV as previously thought, interest in studying the properties of InN has significantly increased. During the last two years a large number of papers devoted to the growth and characterization of InN have been published (for a review see Ref. 2). Nevertheless, the question about the true fundamental band gap E_g and the effective mass at the conduction-band minimum m_{n0} is still open and is an object of intensive theoretical calculations[3,4] and experimental investigations.[5–12] The difficulties for a precise determination of the band gap from the absorption and photoluminescence spectra arise from the fact that mostly samples with high doping concentration have been studied where the effects of band filling, band nonparabolicity, and electron-electron and electron-impurity interactions play a significant role and should be properly accounted for. In Ref. 9, a value of $E_g=0.69$ eV has been extracted from the absorption and photoluminescence spectra of samples with carrier concentration $n>6\times10^{18}$ cm^{-3}. The fitting of the spectra has been performed within the band-to-band recombination model with taking into account the Burstein-Moss shift and band gap renormalization due to many-body effects. Although good agreement with experimental spectra was obtained, the value used for the effective mass at the conduction-band minimum, $m_{n0}=0.1m_0$, strongly contradicts the universal Kane's relation ($m_{n0}\sim E_g$) predicting a band gap energy of 1.7 eV if $m_{n0}=0.1m_0$ or, alternatively, a much lower effective mass ($m_{n0}=0.042m_0$) is expected if the band gap is near to 0.7 eV.[13] The same value of the band gap ($E_g=0.69$ eV) has been obtained in Ref. 12 by fitting the absorption spectra in a lightly doped sample ($n=3.5\times10^{17}$ cm^{-3}) with a sigmoidal function which includes only the band tailing effect and does not involve any value for the effective mass. These authors pointed out that the energy position of the photoluminescence peaks cannot be used for determining the fundamental band gap. Recently, improved technology[14] has allowed a growing of InN epitaxial layers with relatively low electron concentration, high crystalline quality, and well-defined light emission spectra. In addition, some detailed investigations of the electrical properties[15,16] of InN give an opportunity for a more precise quantitative interpretation of near-band-edge luminescence spectra.

In this work, we study the low-temperature emission of epitaxial InN layers with carrier concentration in a range 7.7×10^{17}–6×10^{18} cm^{-3}. We interpret the emission spectra of such highly conducting layers in terms of the free-electron recombination band (FERB) model, previously introduced for other III-V highly doped semiconductors—i.e., GaAs,[17,18] InP,[19] InSb,[20] and GaN.[21] Analyzing simultaneously the shape and energy position of the emission spectra and taking into account specific peculiarities at both high and low doping levels we are able to determine the fundamental band gap for the electron effective mass in InN, which is found to satisfy Kane's relation.

The samples we investigate are grown on (0001) sapphire with AlN or GaN buffer layers by molecular beam epitaxy (MBE) (samples 1–3) and metalorganic vapor phase epitaxy (MOVPE) (sample 4). The samples are not intentionally doped having Hall-effect-measured electron concentrations

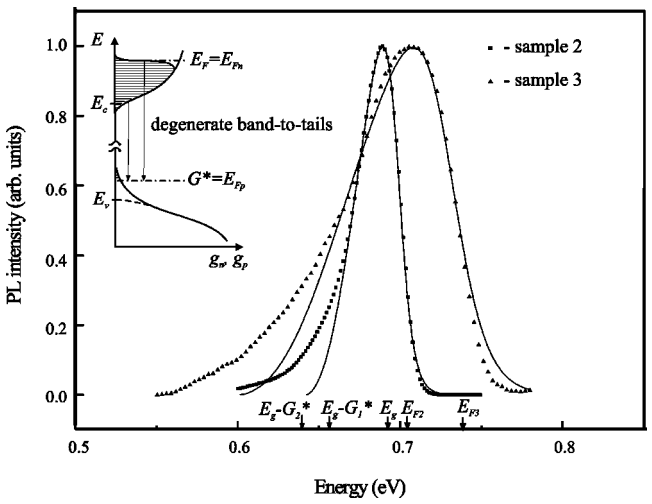

FIG. 1. Experimental (symbols) and calculated (solid lines) PL spectra of samples 2 and 3. The inset schematically shows recombination mechanism of degenerate electrons from the conduction-band DOS to the level G^* in the valence-band tails as used in the modeling. The energy positions of the best-fit values of E_g, E_F, as well as of the unperturbed conduction-band bottom E_g-G^* are also shown.

in the range $n_H=(7.7\times10^{17}-6\times10^{18})$ cm^{-3} and thickness between 0.2 and 1.5 μm (Table I). The details of the growth process as well as some structural characteristics have been published elsewhere.[14,22] It should be noted that the measured Hall concentrations are averaged on the sample thickness and hence they could differ significantly from the values near the samples surface,[23] which are in fact responsible for the emission spectra recorded.

The photoluminescence (PL) measurements are performed at $T=2$ K with an excitation by a continuous-wave Ti:sapphire laser ($\lambda_{exc}=750$ nm) or Ar laser ($\lambda_{exc}=514.5$ nm). Low excitation intensity is used in order to ensure a nonequilibrium carrier density much lower than the doping concentration. The signal is detected by a BOMEM DA8 Fourier transform infrared spectrometer equipped with a liquid-nitrogen-cooled InSb detector. All samples show emission bands around 0.7 eV. No emission at higher energies is observed when exciting with the Ar laser.

PL spectra of samples 2 and 3 are plotted in Fig. 1 (points). They both reveal a broad emission band with a maximum at 685 meV and 705 meV, respectively. The emission band of the sample with a higher Hall concentration of electrons (sample 3) is broader, more asymmetric, and peaked at a higher energy position due to the stronger Burstein-Moss shift. Simultaneously the low-energy side of the spectral band shifts to lower energy compared to sample 2, narrowing the optical band gap. Emission spectra with such a behavior versus carrier concentration are typically observed in highly conducting semiconductors[17–21] and they are characteristic for ''free-to-bound'' radiative recombination of degenerate electrons from the conduction band with nonequilibrium holes located in the valence-band tails (see the inset in Fig. 1). The shape of the emission bands in these spectra closely reproduces the energy distribution of electrons in the conduction band, while their energy positions are determined by the interplay between the equilibrium Burstein-Moss shift and the effective band gap renormalization.

In order to extract analytically the band gap energy we simulate the experimental emission spectra using the general expression for the intensity versus the photon energy $I(h\nu)$ neglecting the energy dependence of the probability for radiative transitions:[21]

$$I(h\nu)\sim\int_0^\infty\int_0^\infty g_n(E_n)f_n(E_n-E_{Fn})g_p(E_p)f_p(E_p-E_{Fp})\times\delta(E_n-E_p-E_g-h\nu)dE_n dE_p. \quad (1)$$

Here $g_n(E_n)$ and $g_p(E_p)$ are the density of states (DOS) in the conduction and valence bands at electron and hole energies E_n and E_p, respectively, f_n and f_p are their nonequilibrium Fermi-Dirac functions, E_{Fn} and E_{Fp} are the quasi-Fermi levels, and E_g is the fundamental (intrinsic) band gap in the ''pure'' semiconductor. The energy-dependent conduction-band density of states $g_n(E_n)$, as well as the corresponding electron effective mass $m_n(E_n)$, is calculated in the framework of Kane's two-band $\mathbf{k}\cdot\mathbf{p}$ model following Ref. 11. In the nonequilibrium Fermi-Dirac function of electrons f_n in Eq. (1) we use the Fermi level $E_{Fn}\approx E_F$ corrected for (i) the temperature of electrons θ, which can differ from the lattice temperature T, (ii) for electron-electron and electron-impurity interactions,[21] and (iii) the nonparabolicity of the conduction-band DOS, which we also calculate in framework of the two-band $\mathbf{k}\cdot\mathbf{p}$ model. The valence-band DOS $g_p(E_p)$ is replaced by a Gaussian determining the tails deep in the band gap through the root-mean-square (rms) impurity potential G (Ref. 21):

$$G=2\sqrt{\pi}\,\frac{4\pi e^2}{\varepsilon R_s}(N_i R_s^3)^{1/2},\quad R_s\cong\frac{a_{Be}}{2}(n a_{Be}^3)^{-1/6},$$

$$a_{Be}=\frac{\varepsilon}{4\pi e^2}\,\frac{h^2}{4\pi^2 m_{n0}}. \quad (2)$$

Here ε is the electric permitivity, R_s is the Thomas-Fermi screening length, $N_i=[(1+K)/(1-K)]n$ is the total ionized impurity concentration, K is the compensation ratio, n is the extrinsic electron concentration, and a_{Be} is the effective Bohr radius of electrons. The value of R_s is smaller than a_{Be} and thus the degenerate electrons (both equilibrium and nonequilibrium) are free above the unperturbed bottom of the conduction band.[21] The situation with the nonequilibrium holes is opposite; in III-V materials the effective Bohr radius a_{Bh} is much smaller than R_s due to the larger effective mass m_p and the holes are, at least at not extremely high impurity concentrations and high temperatures, classically localized[24] in the potential minima of the valence-band tails near the thermal-equilibrium level $G^*=-Ev+\sqrt{2}G-kT/2$. As shown previously,[21] the level G^* plays role of the quasi-Fermi level in the nonquasiequilibrium recombination FERB model and thus we can replace the value of E_{Fp} in the Fermi-Dirac function for holes f_p by G^*—i.e., $E_{Fp}\equiv G^*$. Since the nonequilibrium holes are located in the relatively narrow en-

TABLE I. Carrier concentrations of the samples measured by the Hall effect and parameters obtained from the best fit of emission spectra in the FERB model with effective mass $m_{n0}=0.042m_0$.

Sample No.	n_{Hall} (cm^{-3})	n_{opt} (cm^{-3})	E_g at $K=0$ (meV)	K	G^* (meV)	$E_{F(opt)}$ (meV)
1	7.7×10^{17}		692-60		13.5	
2	1.7×10^{18}	3.6×10^{17}	690	0.06	28.5	35.5
3	6.0×10^{18}	2.0×10^{18}	692	<0.01	55	93
4	6.0×10^{18}	6.6×10^{18}	692+24	<0.01	94	164

ergy interval deep in the band tails, they do not affect significantly the spectral distribution of the emitted light. Therefore, the quantity $g_n(E_n)f_n(E_n-E_{Fn})$ in Eq. (1) nearly reproduces the shape of the FERB according to the upper part of the inset in Fig. 1. The term $g_p(E_p)f_p(E_p-E_{Fp})$ in Eq. (1) determines mainly the energy position of the emission band related to the unperturbed fundamental band gap E_g via Eq. (2) (see the lower part of the inset in Fig. 1). So the FERB model includes a calculation of the spectral shape as well as analytical renormalization of the band gap due to the presence of ionized impurities. In this case the energy positions of both low- and high-energy slopes of the emission band are sensitive to the electron (namely, ionized impurity) concentration.

Further, we simulate the FERB emission spectra of samples 2 and 3 varying n, θ, and K and using the suggested in Ref. 13 value of the electron effective mass at the conduction-band minimum of $m_{n0}=0.042m_0$. For the static permitivity the value of $\varepsilon=14.61\varepsilon_0$ is used,[25] where ε_0 is the permitivity of free space. Assuming a zero compensation ratio (first-order approximation), the best fits of the spectra are satisfied by values of the band gap of 690 meV and 692 meV, for sample, 2 and 3, respectively. The best-fit values of electron concentration and band gap resulting from the modeling at $K=0$ are listed in Table I. Aiming at the best-fit procedure simultaneously for the two samples with the same values of the band gap and the effective mass, we introduce small compensation ratios of $K=0.06$ for sample 2 and $K<0.01$ for sample 3 and obtain $E_g=692$ meV for both samples. The best fits for samples 2 and 3 are shown in Fig. 1 (solid lines). The obtained compensation ratios seem to be realistic[15] and show that the simulation procedure is sensitive even for such low values of K. It is seen from Table I that the best-fit values of the electron concentration n_{opt} are noticeably lower than the Hall-effect-measured ones; however, they still correspond to a degenerate case since the Mott's transition concentration is estimated to be about $n_{\mathrm{Mott}}=5\times10^{16}$ cm^{-3} for $m_{n0}=0.042m_0$. A possible reason for the difference between the Hall and optical values is most likely related to the thickness inhomogeneity of the electrical parameters of the layers, as published previously for similarly grown InN layers.[23] We note that the calculated curves match very well the experimental spectra except for the lower-energy range at low intensity. In this region, a contribution of additional deeper emissions could be expected, as discussed below. Neglecting these emissions in the model does not decrease its accuracy since the main contribution in the analysis is given by the high-intensity part of the emission spectrum, in contrast to modeling of the absorption spectra, where the low-intensity part is used. Thus, a further precise calculation procedure, accounting for all fine effects, could in principle ensure the best possible accuracy.

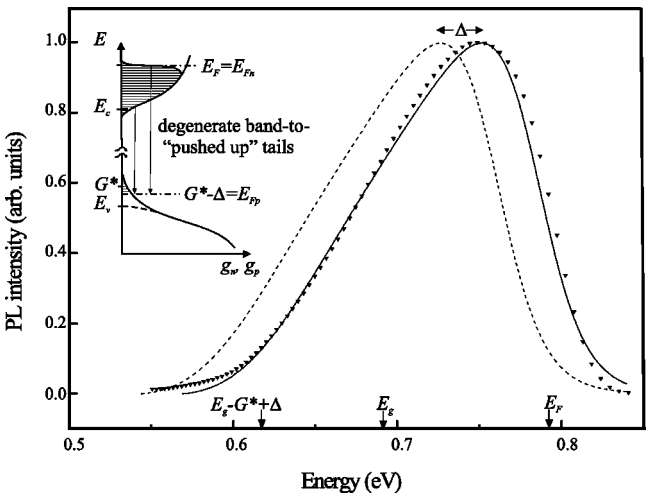

FIG. 2. Experimental PL spectrum of sample 4 (symbols), calculated spectrum in the framework of the FERB model (dashed line) and corrected spectrum by Δ due to the high doping (solid line). The inset represents the recombination mechanism of the FERB model "pushed up" from the level G^*.

The emission spectrum of sample 4 (Fig. 2, points) is broadened and centered at higher energy compared to the spectra of samples 2 and 3. The linewidth corresponds to a higher optical concentration determined in frames of the FERB model (see Table I). Simulating the FERB energy position and assuming the same fundamental band gap $E_g=692$ meV and $m_{n0}=0.042m_0$ we found that the calculated spectrum (dashed line) corresponds in shape to the FERB model but it shows a low-energy shift of about $\Delta=24$ meV compared to the energy position of the experimental spectrum. A possible explanation of this shift is that at very high electron concentration the screening radius R_s becomes smaller even than the effective Bohr radius of holes, a_{Bh}, and the nonequillibrium holes are pushed up over the recombination level G^* in the valence-band tails (see the lower part of the inset in Fig. 2). Further, assuming that the optically estimated electron concentration $n_{opt}=6.6\times10^{18}$ cm^{-3} of sample 4 (see Table I) is near the limit when $R_s\leqslant a_{Bh}$, we estimate the value of the effective Bohr radius of holes, $a_{Bh}\approx2.6$ nm, which leads to a hole effective mass of about $m_p=0.3m_0$.

Figure 3 shows the measured PL spectrum of sample 1 with the lowest doping level (points). It consists of two bands: a high-energy band A_1 centered at 672 meV and low-energy one A_2 at 605 meV. The emission spectrum of sample 1 does not satisfy the FERB model. First, we observe a discrepancy in the shape and low-energy shift of about 60 meV of the band A_1 related to the calculated energy position for "band-to-tails" recombination (dotted line). Second, the full width at half maximum (FWHM) of the experimental band corresponds (if one assumes a FERB) to a rather low electron

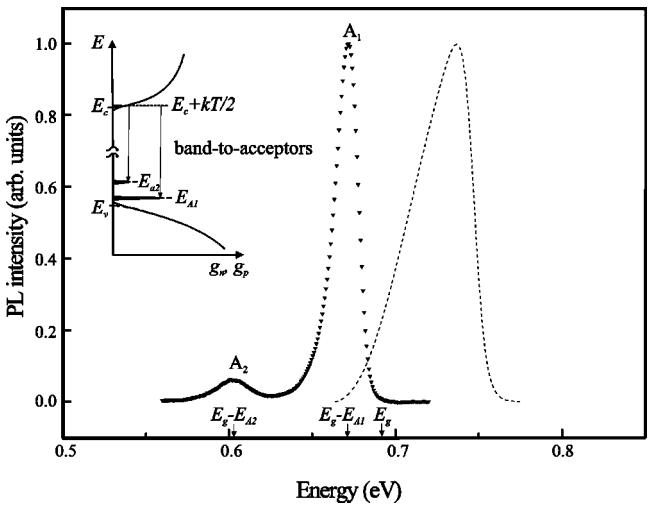

FIG. 3. Experimental PL spectrum of sample 1 (symbols) and the spectrum calculated in the framework of the FERB model (dashed line). The inset shows the recombination paths of band A_1 and band A_2 via shallow and deeper acceptors, respectively, used to explain the experimental spectrum. The arrows show the position of E_g, as well as the values of E_{A1} and E_{A2} related to the band edge.

concentration of about 6×10^{16} cm^{-3} and the electrons near the emitting surface of the sample should not be degenerated even at the assumed low effective mass. In order to resolve the possible recombination path of band A_1 we estimate in the approximation of a simple hydrogenlike model the binding energy of the donor for electron effective mass $m_{n0}=0.042m_0$. We obtain $E_D=2.66$ meV and $a_{Be}=18.4$ nm according to Eq. (2). Such an extremely shallow donor state makes it practically impossible to assume any donor-related recombination in the investigated samples. So based on the performed analysis of the experimental emission spectra, we recognize the two bands observed in the emission spectrum of the sample 1 as resulting from transitions of nondegenerate electrons near the bottom of the conduction band to two acceptor levels: A_1 (shallow) and A_2 (deeper). Having in mind that the maximum of such an emission band corresponds to the difference between the band gap and acceptor binding energy ($E_{\max}=E_g-E_A+kT/2$) we estimate the binding energy of the proposed shallow acceptor A_1 as $E_{A1}=18$ meV, in very good agreement with the value of 20 meV of the calculated binding energy of a hydrogenlike shallow acceptor with the above estimate effective mass ($m_p=0.3m_0$). A deeper acceptor of $E_{A2}=85$ meV can be responsible for the lower-energy emission band (see the inset in Fig. 3). The assumption of the presence of residual acceptors agrees with the anticipated compensation introduced in the simulations of the FERB model for samples 2 and 3. Moreover, the low-energy slope of the emission band of sample 3 is positioned in intensity over the calculated FERB curve, which could result from an overlapping with the A_2 emission. In order to verify the assumed recombination path of the emission band A_1 we run the calculation procedure assuming different values of the electron effective mass $m_{n0}=(0.03-0.15)m_0$ and/or varying the electric permitivity down to $\varepsilon=9.5\varepsilon_0$. Both variations lead to a higher donor binding energy (up to 16 meV) but simultaneously to a stronger increase of the band gap (up to 760 meV) and thus to a greater difference between the band gap energy and peak A_1, making its explanation via ''donor-to-band'' recombination even more contradictional.

For completeness of the analysis we performed modeling of all the spectra varying the effective mass value from $0.03m_0$ to $0.15m_0$. It was found that the larger values of m_{n0} yield a larger spreading of the fundamental band gap for different samples—e.g., $E_g=700-710$ meV—assuming $m_{n0}=0.10m_0$, while for $m_{n0}<0.04m_0$ an unrealistic low electron concentration ($n<10^{15}$ cm^{-3}) is obtained. Thus, we tend to prefer $m_{n0}=0.042m_0$ as a more realistic value for the effective mass at the conduction-band minimum, which results in an analytically estimated fundamental band gap energy of 692 meV, in very good agreement with the value of 690 meV extracted from the absorption spectra.[9,12] Moreover, this value in turn follows the universal $m_{n0}\sim E_g$ relation for Kane's parameter of 14.6 eV.[26] In Ref. 11, a larger value ($m_{n0}=0.07m_0$) has been estimated from the free-carrier plasma reflection but assuming Kane's parameter of 10 eV instead. It is worth noting that due to the strong nonparabolicity of the conduction-band DOS, the accuracy of the experimental determination of the electron effective mass m_{n0} by the optically measured parameters in such highly unintentionally doped samples is, in principle, very low.

We mention that in order to make the accordance between the experimental and calculated spectra even better, several questions have to be further considered like the effect of strain, temperature, etc., but in our opinion they all, in principle, do not discredit the model described here. Also, the model seems to be applicable to explain most of the emission spectra of InN reported recently in the literature after taking into account the respective corrections needed for any specific set of samples. For instance, our temperature-dependent measurements on sample 4 (not shown here) fully agree with the results in Refs. 7 and 12; namely, the PL peak energy shows a very weak (about 8 meV) blueshift with increasing temperature from 2 K to 100 K. Emission spectra with the same behavior have been reported for GaAs in Ref. 18. In our opinion this shift is not unexpected for the FERB emission.[17,21] It can result from an increase of the emitted photon energy due to the temperature-induced pushing up of the nonequilibrium holes located in the valence-band tails. In addition, a decrease of the effective mass with increasing temperature (observed, for example, in GaAs) could increase the Fermi level in the degenerate samples. Both effects are opposite to the commonly observed redshift of the band gap with temperature.

In conclusion, we investigated the shape and energy position of the near-band-edge PL spectra of InN epitaxial layers with different doping levels. The spectra were interpreted by a ''free-to-bound'' recombination mechanism with specific peculiarities for different carrier concentrations. An analytical model for the line shape of the emission was proposed and as a result of the fitting of the experimental spectra the fundamental band gap of InN was found to be $E_g=692\pm2$ meV for an effective mass at the conduction-band minimum of $0.042m_0$.

[1] S. M. Bedair, in *Gallium Nitride I*, edited by J. I. Pankove and T. D. Moustakas (Academic, San Diego, 1998), Chap. 6.
[2] A. G. Bhuiyan, A. H. Hashimoto, and A. Yamamoto, J. Appl. Phys. **94**, 2779 (2003).
[3] F. Bechstdedt and J. Furthmüller, J. Cryst. Growth **246**, 315 (2002).
[4] S. H. Wei, X. Nie, I. G. Batyrev, and S. B. Zhang, Phys. Rev. B **67**, 165209 (2003).
[5] V. Yu. Davydov, A. A. Klochikhin, R. P. Seisyan, V. V. Emtsev, S. V. Ivanov, F. Bechstedt, J. Furthmüller, H. Harima, A. V. Mudryi, J. Aderhold, O. Semchinova, and J. Graul, Phys. Status Solidi B **229**, R1 (2002).
[6] V. Yu. Davydov, A. A. Klochikhin, V. V. Emtsev, S. V. Ivanov, V. V. Vekshin, F. Bechstedt, J. Furthmüller, H. Harima, A. V. Mudryi, A. Hashimoto, A. Yamamoto, J. Aderhold, J. Graul, and E. E. Haller, Phys. Status Solidi B **230**, R4 (2002).
[7] J. Wu, W. Walukiewicz, K. M. Yu, J. W. Ager III, E. E. Haller, H. Lu, W. J. Schaff, Y. Saito, and Y. Nanishi, Appl. Phys. Lett. **80**, 3967 (2002).
[8] T. Matsuoka, H. Okamoto, M. Nakao, H. Harima, and E. Kurimoto, Appl. Phys. Lett. **81**, 1246 (2002).
[9] V. Yu. Davydov, A. A. Klochikhin, V. V. Emtsev, D. A. Kudrykov, S. V. Ivanov, V. A. Vekshin, F. Bechstedt, J. Furthmüller, J. Aderhold, J. Graul, A. V. Mudryi, H. Harima, A. Hashimoto, A. Yamamoto, and E. E. Haller, Phys. Status Solidi B **234**, 787 (2002).
[10] T. Matsuoka, M. Nakao, H. Okamoto, H. Harima, and E. Kurimoto, Jpn. J. Appl. Phys., Part 1 **42**, 2288 (2003).
[11] J. Wu, W. Walukiewicz, W. Shan, K. M. Yu, J. W. Ager III, E. E. Haller, H. Lu, and W. J. Schaff, Phys. Rev. B **66**, 201403 (2002).
[12] J. Wu, W. Walukiewicz, W. Shan, K. M. Yu, J. W. Ager III, S. X. Li, E. E. Haller, H. Lu, and W. J. Schaff, J. Appl. Phys. **94**, 4457 (2003).
[13] B. R. Nag, Phys. Status Solidi B **237**, R1 (2003).
[14] H. Lu, W. J. Schaff, J. Hwang, H. Wu, G. Koley, and L. F. Eastman, Appl. Phys. Lett. **79**, 1489 (2001).
[15] D. C. Look, H. Lu, W. J. Schaff, J. Jasinski, and Z. Liliental-Weber, Appl. Phys. Lett. **80**, 258 (2002).
[16] E. A. Davis, S. F. J. Cox, R. L. Lichti, and C. G. Van der Walle, Appl. Phys. Lett. **82**, 592 (2003).
[17] B. G. Arnaudov, V. A. Vilkotskii, D. S. Domanevskii, S. K. Evtimova, and V. D. Tkachev, Fiz. Tekn. Poluprovodn. **11**, 1799 (1977) [Sov. Phys. Semicond. **11**, 1054 (1977)].
[18] J. De-Sheng, Y. Makita, K. Ploog, and H. J. Queisser, J. Appl. Phys. **53**, 999 (1982).
[19] M. Bugajski and W. Lewandovski, J. Appl. Phys. **57**, 521 (1985).
[20] N. S. Averkiev, B. N. Kalinin, A. V. Losev, A. A. Rogachev, and A. S. Filipenko, Phys. Status Solidi A **121**, K129 (1990).
[21] B. Arnaudov, T. Paskova, E. M. Goldis, S. Evtimova, and B. Monemar, Phys. Rev. B **64**, 045213 (2001).
[22] S. Yamaguchi, M. Kariya, S. Nitta, T. Takeuchi, C. Wetzel, H. Amano, and I. Akasaki, J. Appl. Phys. **85**, 7682 (1999).
[23] V. Cimalla, Ch. Förster, G. Kittler, I. Cimalla, R. Kosiba, G. Ecke, O. Ambacher, R. Goldhahn, S. Shokhovets, A. Georgakilas, H. Lu, and W. Schaff, Phys. Status Solidi C **0**, 2818 (2003).
[24] B. I. Shklovskii and A. L. Efros, *Electronic Properties of Doped Semiconductors* (Springer-Verlag, Berlin, 1984), Chap. 11.
[25] F. Bernardini, V. Fiorentini, and D. Vanderbilt, Phys. Rev. Lett. **79**, 3958 (1997).
[26] I. Vurgaftman, J. R. Meyer, and L. R. Ram-Mohan, J. Appl. Phys. **89**, 5815 (2001).